On the use of geophysical methods for the characterization of earth dams: A case study on the Canal du Centre (France)

Grégory BIÈVRE
Laboratoire régional des Ponts et Chaussées d'Autun

Christophe NORGEOT
DESS - Applied geophysics, Université Paris VI

INTRODUCTION

For many years, residents of the village of Rémigny (in France's Saône-et-Loire department; see Fig. 1), located near the base of the earth dam built along the Canal du Centre (on the valley side), have suffered from repeated water infiltrations. These events may be observed down-slope of the earth dam as well as within several homes.

A visual inspection of the canal, conducted by the company ISL [ISL, 1994], has indicated that the canal is not the sole source of the leaks observed in the dam and that the water table also plays a role. Two complementary observations would serve to substantiate these indications:

- the flow rate from leakage varies with respect to rainfall, even though the water level of the canal remains constant;
- infiltrations within the canal are present on the right bank, i.e. the hill side; the origin of this water must thus stem from the water table.

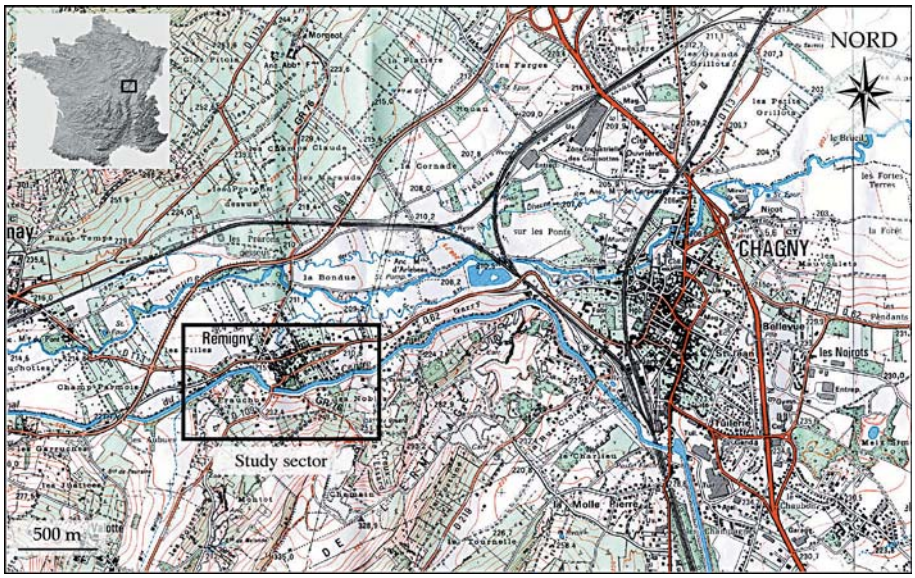

Figure 1
Geographic location of the study sector

It is still difficult however to determine the appropriate breakdown (leak flows generated by the canal *versus* the water table), given that no piezometric monitoring has been performed since the ISL study in 1994. Fluorescein tracing tests, carried out at the level of the two down-slope leakage zones, reveal that the leaks present are due to the canal and provide a source of inflow as well.

It appeared necessary to get information on the stratigraphic, structural and hydrogeological organization of this part of the canal, in order to better assess the proportion of water from the canal causing infiltration inside residences. Within the scope of this study, reconnaissance campaigns using geophysical methods (radio-magnetotellurics) were utilized, and boreholes were drilled for purposes of method calibration [Rousseau and de Sambucy, 1993]. Following a data synthesis stage [Norgeot, 2000], which incorporated data from both mechanical and radio-magnetotelluric (RMT) probes, other prospection campaigns were conducted (refraction seismics, subaquatic resistivity profiling, ground-penetrating radar).

This article presents a summary of the non-destructive geophysical methods implemented on this site and identifies those that have yielded interpretable results. The results obtained from testing using an aquatic streaming of spontaneous potential (SP) method [Norgeot, 2000] will also be highlighted. This work, which lies fully within the scope of a number of current research topics [Mériaux *et al.*, 2001; Fauchard and Mériaux, 2004], demonstrates the benefit of performing a detailed geological and structural study prior to conducting evaluations and measurements on the actual structure whenever it is intimately tied to the surrounding geological setting.

In the following discussion, the word "infiltration" denotes any inflow of groundwater towards the canal and "leakage" refers to any loss of water from the canal towards the exterior (via either the body of the earth dam or the substratum).

GEOLOGICAL AND HYDROGEOLOGICAL FRAMEWORK

The study sector is located in the village of Rémigny, close to the city of Chagny (see Fig. 1). The Canal du Centre follows the course of the Dheune river valley and, at the level of the study zone, is situated at the base of the hillside; it has been built with a mixed profile, i.e. cut on the hillside and fill on the valley side (see Fig. 2).

The morphology of the region indicates two major realms. The first one, on the western part, consists in a limestone plateau that overlooks the second one, the Bresse plain, located to the east. This limestone plateau is cut off by the Dheune river valley that joins the Morvan region to the Saône river plain.

The limestone strata of the study sector are dated from the middle and upper Jurassic (Figs. 3 and 4); these are rather massive carbonate strata, with distinct stratification, deposited within a relatively shallow setting (many oolitic levels, oblique stratifications), alternating with marly formations (*Digonella*-rich callovian marls, middle and upper oxfordian marls). The plain is composed of fluvio-lacustrine and fluviatile formations that are being deposited since the Cenozoic within the Bresse trench. The bases of the slopes are made up of slope rubbles and colluvia.

From a structural point of view, the tectonical setting of the region is principally linked to the alpine tectonic phase. These movements were active during the wole Cenozoic; several phases, especially during the "Oligocene crisis", contributed to the deepening of the Bresse trench. The entire series of carbonate strata have thus been cut and dip now to the east.

In the specific case of our study sector, the Dheune river valley constitutes a structural hinge at a regional scale (Fig. 3a). To the north lies the "Arrière-Côte" system, made up of a series of faulted tabular or monoclinal plateaus arranged as downstepped blocks dipping to the east. To the south of the Dheune river valley, the jurassic plateaus correspond to the faulted monoclinal structure of the Chalonnais zone, arranged in narrow strips separated by faults and gently dipping to the east-southeast (approximately 5°). This structural unit dips below the Bresse plain to the east (Fig. 3). The Dheune river valley is the result of the reactivation of a variscan senestrian strike-slip fault [Rat, 1986] that delimits the northernmost part of the Blanzy Basin, and which had a motion [a N60-70°E orientation; Fleury and Gélard, 1983].

The two levels that form the geological substratum of the Canal du Centre in the study area are: 1) the 25 m thick upper Bathonian and Callovian carbonate strata (from bottom to top: "Grenu inférieur", Digonella divionensis marls, "Grenu supérieur", striped cherty limestones and nodular clayey limestones); and 2) the 50 m thick Saint-Romain limestones (Figs. 3b and 4).

These two formations are separated by a fault, labelled F1 on Figure 3b, oriented N40-45°E, with a downward motion of the block located to the west. At the end of the zone, to the east, a second vertical fault, labelled F2 on Figure 3b, with the same direction as F1, places the Saint-Romain limestones into contact with the upper Bathonian and Callovian limestones, dipping to the east.

Both sedimentary configuration (stratified carbonate strata) and morphotectonic structural patterns (narrow strips dipping eastwards, along with a high level of fractures) favor the presence of aquifers within these Jurassic strata (karstic levels), with water flows being quickly routed towards a fracture. At the base of the Nantoux limestones (Fig. 4) for example, which is more or less dolomitized, several grottoes formed in the region [Fleury and Gélard, 1983]. Furthermore, according to the geological map, it appears that the canal, in the study area, would have been partially constructed along the two faults F12 and F2 (Fig. 3b).

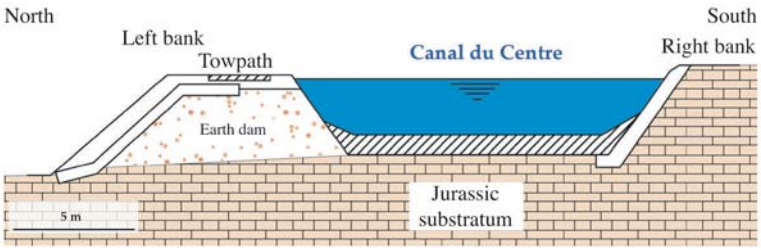

Figure 2

Transverse section cut of the Canal du Centre at the level of the study sector: Modified after ISL [1994]

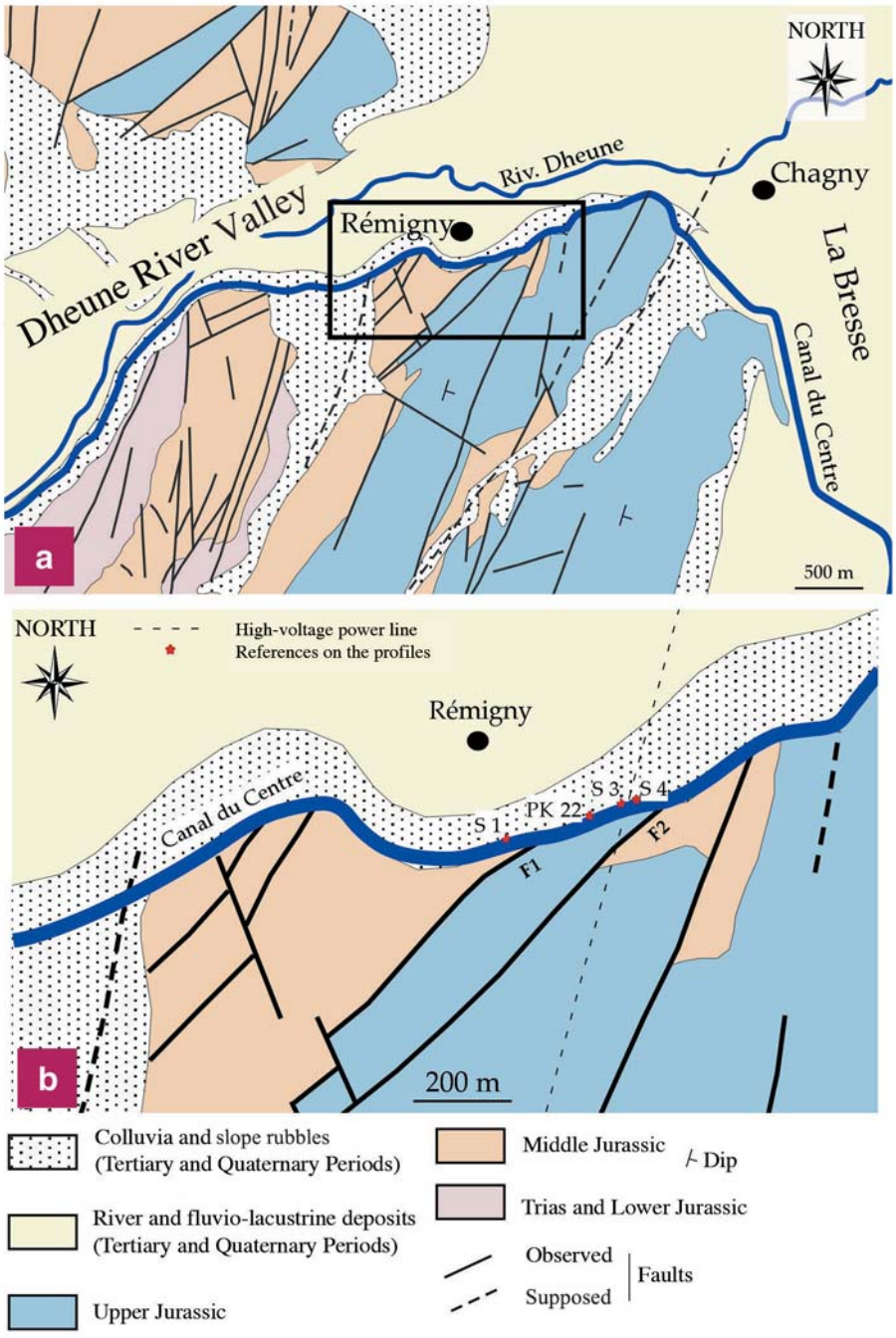

Figure 3

Geological setting of the study sector [extracted from Fleury and Gélard, 1983]:
a. Regional structural diagram
b. Close-up of the study sector and position of the reference points

Study methods and results

Physical measurements on various water samples

Point-specific measurements on water samples were performed at various locations: the canal, wells, drains, boreholes, infiltration water and source water. Three sampling series were carried out in July 1996, October 1996 and January 1997 [Archambault, 1997]. Three parameters were measured in

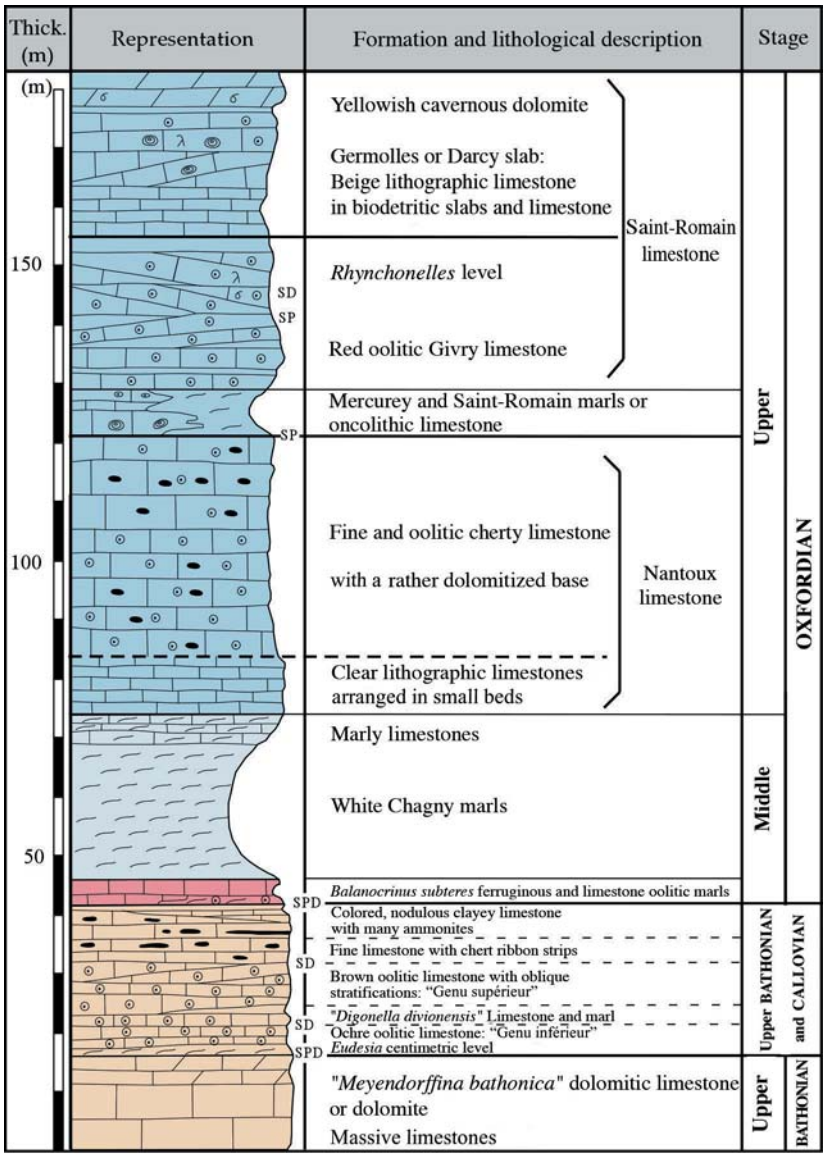

Figure 4

Lithostratigraphic log of the strata encountered [after Fleury and Gélard, 1983]. SD: hardened surface, SP: perforated surface, SPD: hardened perforated surface.

an attempt to characterize the leakage water and its origin: groundwater, canal water, or both. These parameters are as follows:

- electrical conductivity, which represents the ease with which electrical current is able to circulate. This parameter is expressed herein in microSiemens per centimeter (µS/cm);
- water temperature, expressed in degrees Celsius (°C); and
- pH.

The maps (Fig. 5) display the measurements conducted in July 1996, plus the temperature measurements from January 1997. The density of measurement points and the place of water extraction (i.e. drain, canal, borehole, source, well) have all been indicated on this same figure. Dummy points, labeled "PF" with the same characteristics as canal water, were added to the representation in order to depict the path taken by canal water; interpolation was performed by means of triangulation.

Observations of these maps enabled detecting the presence of several types of water on the basis of physical characteristics. For the month of July 1996, a low-conductivity water was determined (less than 450 µS/cm), along with high temperature (above 21°C) and a pH in the vicinity of 7.5. It was then possible to discern a high-conductivity water (greater than 500 µS/cm), associated with lower

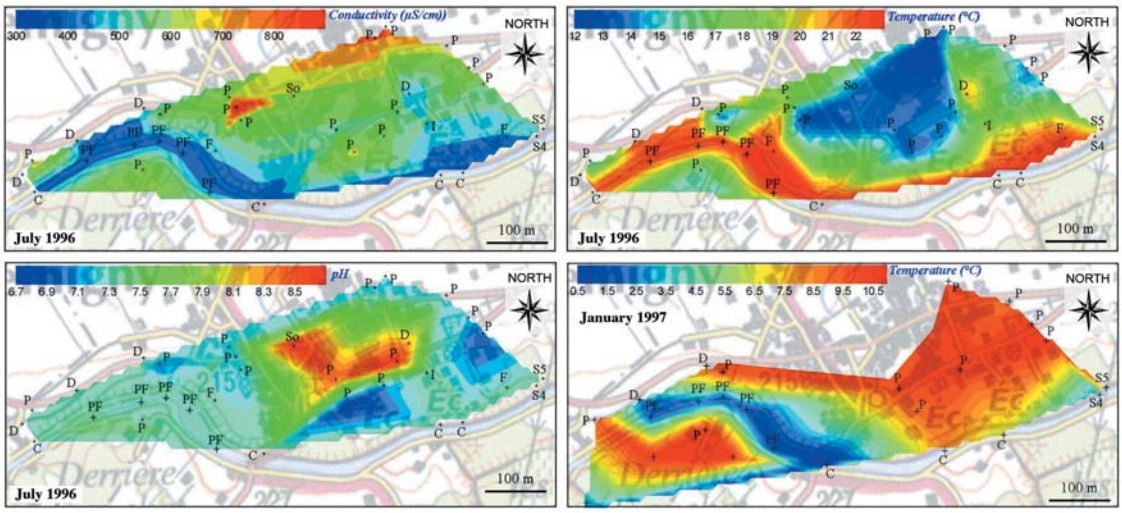

Figure 5

Physicochemical measurements from July 1996 and October 1997 [data extracted from Archambault, 1997]: C: canal; D: drain; I: average of infiltrations inside residences; P: wells; S_n: piezometer in borehole; So: source; PF: dummy point

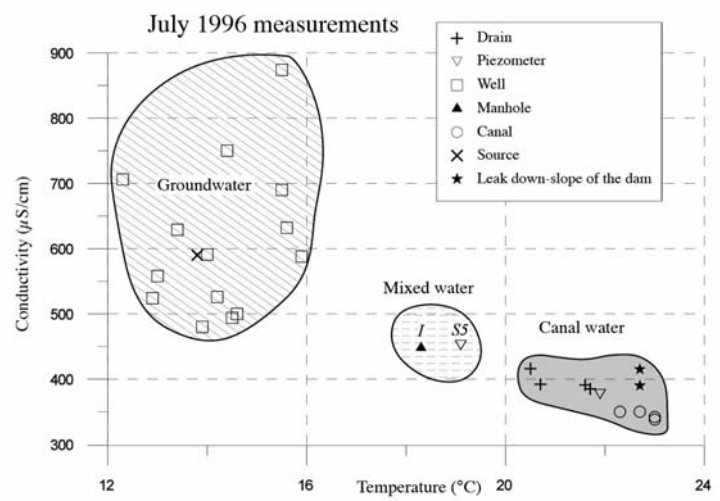

Figure 6

Conductivity-temperature diagram based on the physicochemical measurements from July 1996 [data extracted from Archambault, 1997]. The analysis of this diagram enables distinguishing three types of water corresponding to canal water, groundwater and an intermediate water between these two (mixed water).

temperature (below 17°C) and a pH exceeding 7.5. These two types of water correspond respectively to the canal water, with higher temperature (summertime surface water), and to groundwater, featuring lower temperature, due to its position within the substratum and with high conductivity given that it can be ion-charged when crossing the aquifer. The pH values do not allow undertaking the same kind of differentiation.

The temperature map from January 1997 allows to distinguish two water sources, with the temperatures being (logically) distributed inversely with respect to the summer season (Fig. 5): canal water in this case is colder than groundwater.

An initial analysis of these maps reveals that some of the measurements conducted in wells (and thus most likely on groundwater) exhibit the same characteristics as those carried out on the infiltration water inside the residences. Similarly, the infiltration water presents the same characteristics as the canal water. These results tend to indicate a mixed origin for the infiltration water.

The creation of a diagram of temperature *vs.* conductivity for the July 1996 samples, as shown in Figure 6, enables confirming this initial analysis and highlights a distribution of data points split into three distinct groups. The measurements taken on groundwater (i.e. wells and the source) are characterized by a low temperature (between 12 and 16°C) and high conductivity (450-750 µS/cm).

Conversely, the measurements conducted on canal water show a low level of conductivity (300-425 µS/cm) and warmer temperatures (20-24°C). Two measurements (a temperature of 18 to 19°C and conductivity on the order of 450 µS/cm) suggest an intermediate state, most likely corresponding to a mix of waters stemming from both the water table and the canal. It may also be considered that the proportion of canal water is higher, since the characteristics of these mixed samples lie closer to those of the canal than to those from the water table. This hypothesis however may be altered depending on the speed of canal water flow through the soil via canal leakage.

It is worthwhile to note that the two intermediate points correspond to measurements carried out in a borehole on the banks of the canal and on an infiltration source inside an affected residence. The borehole measurement (reference S5, Figs. 5 and 6) reveals that the earth dam embankment is crossed by canal water as well as by groundwater, with the latter source being the cause of the carbonated formations located on site. The measurement taken on residential infiltration water (reference I, Figs. 5 and 6) indicates that this water is due to a mixed source.

Geophysical methods

Various geophysical methods were employed in an attempt to identify the formations present. Prospections were conducted on the dam body (radio-magnetotellurics, refraction seismics and ground-penetrating radar) or else on the canal floor (subaquatic resistivity profiling). Another technique being developed, which entails the aquatic streaming of spontaneous potentials, has also been introduced; it will be presented following the mechanical boreholes. Figure 7 provides the relative positions of the various geophysical profiles.

The radio-magnetotelluric technique

Two radio-magnetotelluric (RMT) profiles were acquired from west to east over the canal towpath, on the valley side [Rousseau and de Sambucy, 1993; location of profiles on Figure 7]. Credit for discovering this method goes to Cagniard [1953], with the initial application of RMT dating back to the mid-1970's [e.g. Guineau, 1975]. RMT is a low-frequency electromagnetic prospection technique with an emitter placed at infinity; it yields a continuous measurement of the apparent resistivity of the substratum by using civil radio broadcasting emitters whose frequencies lie between 10 kHz and 1 MHz. The waves emitted get propagated through the ground and generate electrical currents by means of induction. These currents may then be connected to electrical and magnetic fields that are measured, for determined frequencies, by a capacitive dipole placed at the ground level and by an inductive coil, respectively. Apparent resistivities are computed by use of Equation (1) below, which governs the magnetotelluric phenomena [Cagniard, 1953]:

$$\rho_a = \frac{1}{2\pi f \mu_0} \left| \frac{E_x}{H_y} \right|^2 \qquad (1)$$

with:

- ρ_a = apparent resistivity (Ω.m),
- E_x = electrical field at the ground surface (V/m),
- H_y = magnetic field at the ground surface (A/m), perpendicular to E_x,
- f = frequency of the selected electromagnetic wave (Hz),
- μ_0 = magnetic permeability of the void (= $4\pi 10^{-7}$ H/m).

The measurement equipment is pulled by a vehicle that travels over the body of the dam. Under easy driving conditions, it is possible to perform several kilometers worth of measurements per day. Results are presented in the form of apparent resistivity profiles (see Fig. 8). Two frequencies were used for this purpose (162 and 603 kHz), with the lower frequency allowing in theory to perform deeper investigations.

The 603-kHz profile shows an average for the entire profile of 36 Ω.m. It then becomes possible to distinguish two groups, on the basis of the "regional variations" analysis [Lagabrielle and Hollier-Larousse, 1985; Hollier-Larousse, 1997], as highlighted by the arrows on Figure 8. These arrows reveal the "trend" in curve shape, i.e. average increase or decrease in the apparent resistivity values. The first sector, from the beginning of the profile until PK 22, exhibits an average apparent resistivity of 30 Ω.m, along with a few local variations of small magnitude (Fig. 8). Beginning at PK 22 and extending until the end of the profile, the average value is 45 Ω.m and the profile contains a few local variations of small magnitude. This profile indicates a compartmentalization into two blocks, with surface terrains on the whole being slightly more resistive as of PK 22.

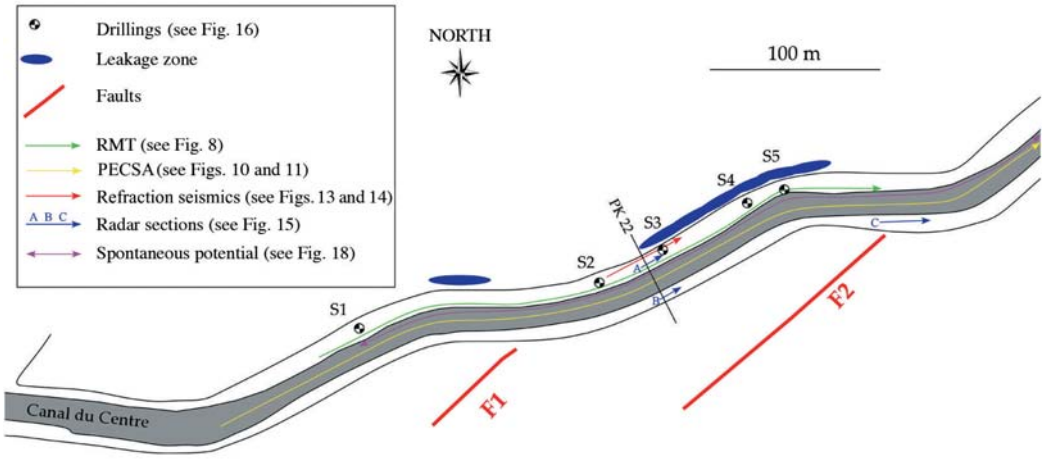

Figure 7
Location of the geophysical measurements

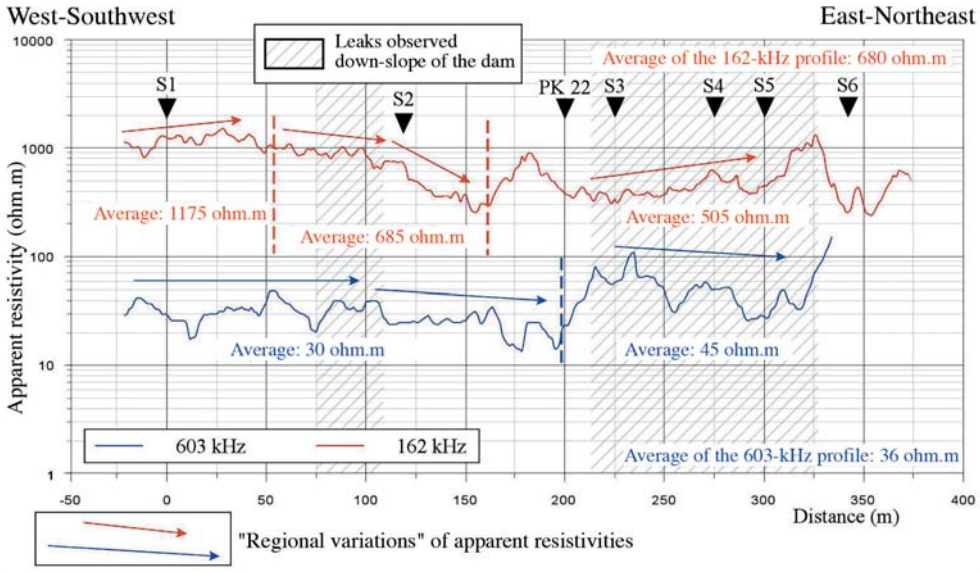

Figure 8
Radio-magnetotelluric (RMT) profiles derived on the crest of the earth dam [modified after Rousseau and de Sambucy, 1993].
The position of the profiles is indicated on Figure 7.
The average apparent resistivity value of each profile is given, as is the average value for each homogeneous zone. Arrows indicate the "regional variations" in apparent resistivities [Lagabrielle and Hollier-Larousse, 1985].

The 162-kHz profile pertains to a more sizable volume of earth and thus corresponds to an ostensibly deeper investigation. The average for the entire profile equals 680 Ω.m. Just as before, it is possible to distinguish three zones on the basis of the lateral variations in apparent resistivities (Fig. 8).

The penetration depth (or "skin depth") is given by Equation (2) [McNeill and Labson, 1991]:

$$z = \sqrt{\frac{\rho}{\pi \mu_0 f}} \approx 503\sqrt{\frac{\rho}{f}} \qquad (2)$$

with:

- z = penetration depth (m),
- ρ = average apparent resistivity (Ω.m),

- μ_0 = magnetic permeability of the void (= $4\pi 10^{-7}$ H/m),
- f = frequency of the electromagnetic wave (Hz).

At 162 kHz therefore, with an average apparent resistivity of the profile at 680 Ω.m (Fig. 8), the penetration depth is approximately 32 m and, at 603 kHz, it lies on the order of 4 m. It is recognized that the depth of investigation *d* equals half the penetration depth. For an acquisition at 162 kHz, the data will thus focus on the geological setting (d =z/2 = 16 m); similarly, the profile at 603 kHz will pertain to those surface levels that constitute the body of the dam (d = z/2 = 2 m).

Recent work [Fauchard and Mériaux, 2004] has demonstrated, however, that this method remains difficult to implement on earth dam structures. At present, the preference tends to favor low-frequency electromagnetic methods (LFEM) of the Slingram type.

Continuous electrical profiling on an aquatic site (PECSA)

The technique applied consists in injecting continuous electrical current, by means of an AB dipole with fixed 10-m spacing, streaming over the bottom of the water flow, and then measuring the potential differences induced via a multi-electrode device NM_x that has also been placed at the bottom of the water [Lagabrielle and Teilhaud, 1981; Lagabrielle, 1983, 1984; Lagabrielle and Chevalier, 1991]. This set-up contains a total of eight measurement electrodes that serve to define seven dipoles, with the biggest featuring a spacing NM_7 of 100 m (see Fig. 9).

For a given PECSA profile, seven apparent resistivities are recorded simultaneously; these serve to define an electrical probe that corresponds to investigation depths increasing from NM_1 to NM_7. The execution of several electrical probes along a profile, as specified in an appropriate sampling step, allows studying vertical and lateral variations in the apparent resistivities of the substratum along this profile. It is then possible to complete, using this method, several kilometers of profiling per day. The computation of apparent resistivities is performed by applying Equation (3) [Lagabrielle, 1984]:

$$\rho_a = k\frac{\Delta V}{i} \qquad (3)$$

with:

- ρ_a = apparent resistivity (Ω.m),
- $k = \dfrac{2\pi}{\frac{1}{AM_i} - \frac{1}{AN_i} - \frac{1}{BM_i} + \frac{1}{BN_i}}$: geometrical factor, function of the measurement device,
- ΔV = measured potential difference (V),
- i = intensity of the injected current (A).

Two apparent resistivity profiles were generated in order to establish the electrical properties of the substratum underneath the canal (see the profile positions on Figure 7). The results obtained are of very good quality and did not require any *a posteriori* filtering. The resistivity of the water, measured by a fully immersed 24 cm long Schlumberger quadripole, is constant over the entire profile (approx-

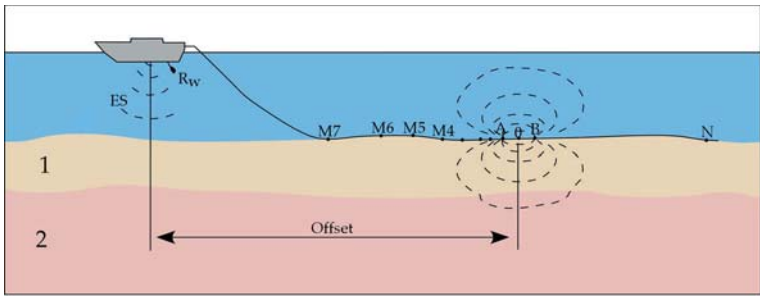

Figure 9

Continuous electrical profiling at an aquatic site. Device for measuring the apparent resistivity of the subaquatic substratum applied here to soils 1 and 2 with respective resistivities of ρ_1 and ρ_2. A, B: injection electrodes – M_x, N: measurement electrodes – R_w: resistivity measurement of water – ES: echo probe, bathymetry measurement – offset: distance between the boat and the center of the measurement device (0), considered here as being located in the middle of injection dipole AB.

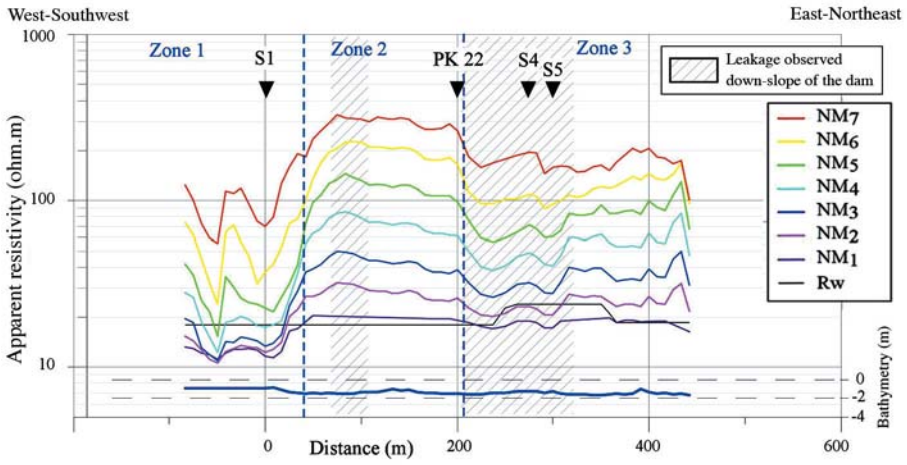

Figure 10

Profiles of apparent resistivity within an aquatic medium [Bièvre, 2002]. Bathymetry: height of water in the canal; R_w: apparent resistivity of water; NM_1 to NM_7: apparent resistivity of the substratum on the basis of increasing measurement electrode spacing from 1 to 7 (NM_1 = 56 m, NM_7 = 100 m). The position of the profiles is located on Figure 7.

imately 20 Ω.m; Fig. 10). Since the two profiles have yielded analogous results, a single profile is presented herein.

The PECSA data provide information on the strata situated below the canal floor and thus below the body of the earth dam. These measurements pertain specifically to the geological setting of the canal. Caution must nonetheless be exercised when proceeding with interpretative assessments; data from the apparent resistivity profiles, which are one-dimensional, actually allow resistivity recordings in three dimensions.

The apparent resistivities lie between 10 Ω.m (NM_1) and 300 Ω.m (NM_7). The measurements are regular and vary in the same direction, as apparent resistivities increase with electrode spacing. An analysis of the profiles leads to defining a compartmentalization of the subaquatic substratum into three primary zones, based on electrical responses. The first zone (start of profile to abscissa x = 40 m) is only slightly resistive, as is the third (beyond PK 22). Between the benchmarks x = 40 m and PK 22, the substratum is more highly-resistive, which seems to indicate that the substratum is more massive and less fractured. This organization tends to be found once again at the end of the profile.

On a given profile, the entire set of electrical soundings have been used to perform inversions, based on Zohdy's method [1989] and implemented according to a computation algorithm developed at the Laboratoire Central des Ponts et Chaussées. To proceed, the measurement of water resistivity as well as bathymetry are necessary, with the water layer being taken as the initial model ground layer [Lagabrielle and Chevalier, 1991]. This step consisted of a one-dimensional inversion that provides for a vertical distribution of apparent resistivities, interpreted as a function of depth. The horizontal assembly of these one-dimensional vertical interpretations in turn yields a two-dimensional vertical section cut; this cut is obtained through use of a computation grid that has been derived herein by means of triangulation with linear interpolation.

The model obtained is indeed consistent with observations stemming from the apparent resistivity profiles: three primary zones may be distinguished on the basis of the electrical properties (see Fig. 11a). It also seems that a dip is present within Zone 3 (from PK 22 extending to the end of the profile). The substratum appears to become more highly resistive towards the end of the profile and once again displays a distribution of the electrical aspect similar to that observed within Zone 2.

The data inversion phase also allows making use of prediction errors, i.e. the average quadratic deviation, from a least squares standpoint, between the experimental measurements and measurements stemming from predictions by the proposed model. It is thus possible to evaluate the degree of consistency between the experimental soundings and the derived model. The computations are carried out on a sounding basis (and therefore independently of one another), and the average quadratic deviation curve undeniably exhibits some resemblance to the apparent resistivity results, i.e. compartmentalization shows up in the same places (see Fig. 11b; the curve represents the average

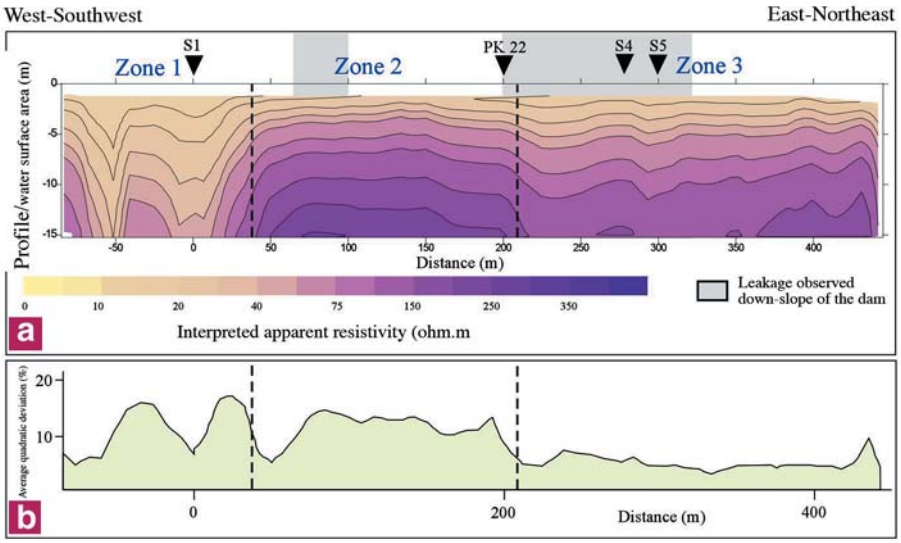

Figure 11 [extracted from Bièvre, 2002]
a. Inversion of the electrical aquatic data and assembly in a two-dimensional profile
b. Average quadratic deviation between experimental measurements and model predictions

quadratic deviation, expressed herein in percentage terms, between experimental measurements and inverse data). It would thus seem that a parameter inherent to the type of soil influences the quality of the model. It is likely that one of the boundary conditions present in the use of this technique, such as the tabularity of substratum formations [Lagabrielle, 1984], is only slightly respected at the beginning of the profile, up through PK 22 (x = 200 m), in light of the divergences existing between the computed model and the electrical probe.

Refraction seismics

In order to generate complementary geophysical data on the body of the earth dam, two refraction seismics profiles were acquired, both of them centered on PK 22, over a linear distance of 45 m (see Fig. 7). This conventional prospection method is based on the study of mechanical wave propagation (compression waves) over the upper part of the substratum when layers are sub-horizontal. A seismic source is created and then moved along a given profile. Various geophones placed along this profile then enable recording the arrival times of the vibrations and building a time-distance curve, referred to as a dromochronic plot (Fig. 12). In refraction seismics, the "first arrival" times are the ones used (i.e. the first vibrations recorded by the geophone once the disturbance had been generated).

In order for the waves emitted from the surface, with an incident angle of i_c, to reach an interface located at depth *Z* and then get refracted along this interface by an angle i_r (i_r = 90°) before being picked up by the geophones at the surface, the medium must allow for the emergence of a refracted ray. The minimum preconditions require both that the stratification fulfills the boundary angle conditions and that Medium 2 enables faster propagation of P-waves than Medium 1 [Keary and Brookes, 1991]. This condition establishes the notion of a critical angle (i_c), which is governed by Equation 4 below and which is also called Snell's law [Keary and Brookes, 1991]:

$$\frac{\sin i_c}{v_1} = \frac{\sin i_r}{v_2} = \frac{\sin 90°}{v_2} = \frac{1}{v_2} \qquad (4)$$

with:

- i_c = critical incident angle (in degrees),
- i_r = angle of refraction (= 90 degrees),
- V_1, V_2 = P-wave propagation speeds within Medium 1 and Medium 2 (in m/sec, with $V_1 < V_2$).

For geophones closest to the source, the direct wave is obviously the quickest. In deviating from this wave, the refracted wave, which reaches the first interface (see Fig. 12: boundary between the surface soils at speed V_1 and the substratum at speed $V_2 > V_1$), then moves more quickly due to a higher

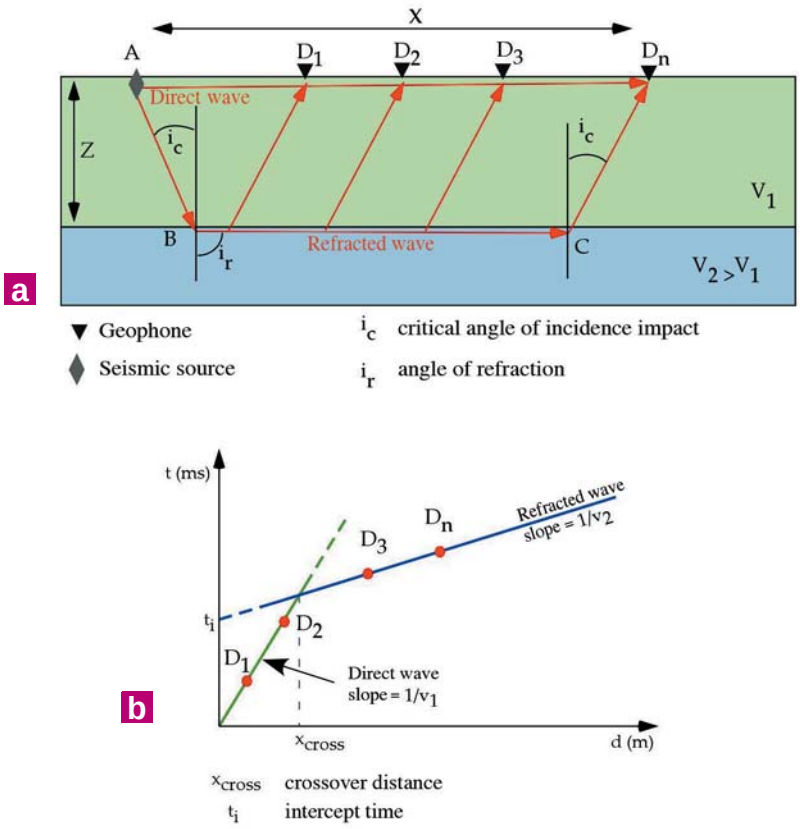

Figure 12

Refraction seismics principle for a tabular medium with two layers 1 and 2 and an increasing distribution of mechanical wave speeds vs. depth ($V_2 > V_1$):
a. Direct and refracted wave path, and simplified data acquisition sketch [adapted from Keary and Brookes, 1991]
b. Construction of the time-distance curve (dromochronic plot) derived from the data presented in a)

propagation speed within this second medium. Beyond a certain distance, called the "crossover distance" (x_{cros} on Figure 12), the refracted wave arrives first at the geophone. Given both distance and time, it becomes possible to compute the propagation speeds of seismic waves within the various layers. Next, by means of geometrical and trigonometric relations (Equations 4 and 5), it is now possible to compute the depths of these interfaces beneath the shots via Equation 5, i.e.:

$$Z = \frac{t_i v_1 v_2}{2\sqrt{v_2^2 - v_1^2}} \qquad (5)$$

with:

- Z = depth of the interface beneath the shot (m),
- t_i = intercept time (s); this parameter reflects the temporal value assumed by the curve with slope $1/V_2$ for a zero distance,
- V_1, V_2 = P-wave propagation speeds within Medium 1 and Medium 2 (m/sec).

Measurements were carried out using an ABEM Terraloc MK3 device that comprises 24 geophones spaced 1 m apart, with both profiles containing two common geophones in order to ensure a good level of overlap. The disturbances were generated using a sledgehammer. It is generally considered that to obtain an accurate characterization of an interface located at depth Z, the surface device must have a length of 4Z. Since the objective herein is to characterize the interface between the body of the earth dam and the substratum, situated between 3 and 6 m (see the section entitled "Mechanical probes"), the device selected displays an inter-geophone spacing of 1 m and a total device length of 23 m. With this equipment layout, an easily-accessible site and two operators, the output stands at approx. 150 to 200 m per day at most, which represents 6 to 8 profiles. The devices were centered on

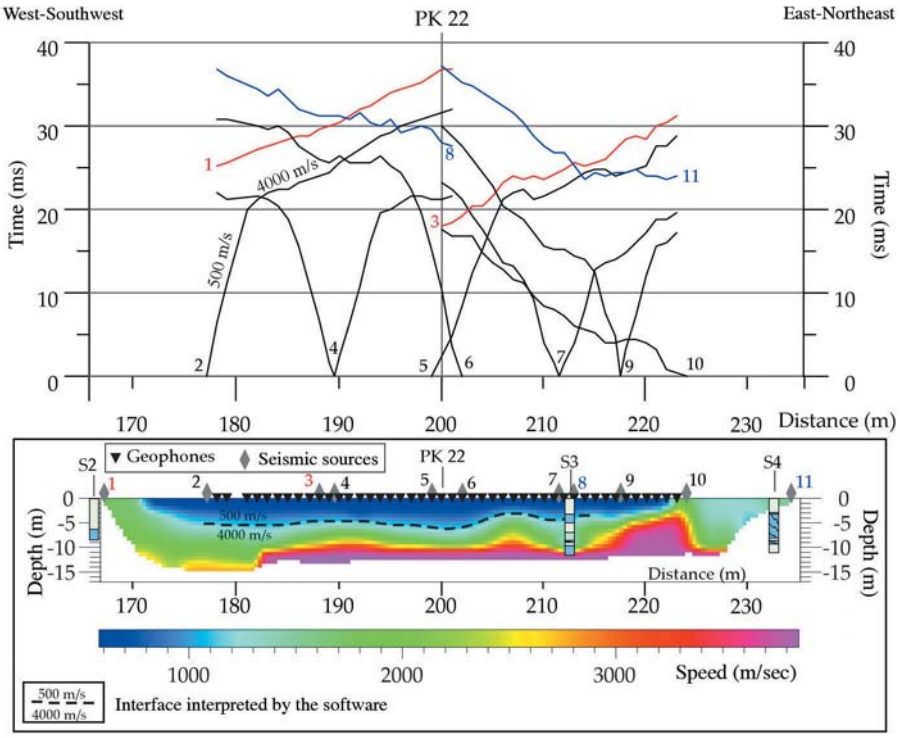

Figure 13

Dromochronic plots and inversion model obtained on the study sector. The labels 1 through 11 indicate the correspondence between the seismic source and the resultant dromochronics. A geophone was not operable and has not been included in the representation (third geophone from the left). The position of the profiles has been indicated on Figure 7 [Document furnished by CETMEF].

PK 22, for the purpose of confirming the lateral variations at this spot observed in aquatic electrics at the substratum level. The dromochronic plots have been represented on Figure 13. Since one of the geophones had not operated correctly (third geophone from the left), its results were not included.

The largest section of the profile indicates a substratum (approx. 4,000 m/sec) located under a cover layer (approx. 500 m/sec) that decreases in thickness eastwards. The dromochronic plot of the shot at the end of the eastern line (shot no. 10 at 224 m) shows that the mechanical waves are directly propagating at a greater speed than that of the waves within the substratum over the remainder of the profile (more towards the west). It is likely that at this particular spot, a zone containing open vertical fractures acts as a waveguide and enables the mechanical waves to reach the substratum under the embankment very quickly. This analysis has been bolstered by observation of the shot at offset no. 11 positioned at 234 m (this shot relates to the substratum situated in alignment with the geophones): the mechanical waves, under this same section of profile, propagate very rapidly and then make their way to a slower medium, most likely corresponding to the substratum. It would thus seem that by the end of this profile, the extreme point is located at the level of a fractured zone.

These data were then processed using the method of simulated annealing [Abbot *et al.*, 2001; Pullammanappallil and Louie, 1994, 1997]. Put succinctly and as opposed to the conventional interface depth computation processes (e.g. the "plus-minus" method [Hagedoorn, 1959]; the reciprocal method [Hawkins, 1961]), this modeling approach more closely resembles a tomographic technique. The seismic profile models are obtained by means of a Monte Carlo-type technique, which consists of a numerical simulation method based on sampling formulae and probabilistic approaches (statistical solution of the direct problem without inversion).

It is merely required therefore to possess the geometry of the shot lines as well as the peak points from the first arrivals (i.e. data that allows constructing the dromochronic plots). The results are presented under the form of an image showing speed variation gradients vs. depth. The interfaces between layers of various speeds can be found where the speed gradient variation is strongest. This application also allows to place the interfaces between the various layers (i.e. an interface between 500 and 4,000 m/sec), after having determined the seismic speeds of these layers (from the dromochronic analysis) and incorporated them into the model.

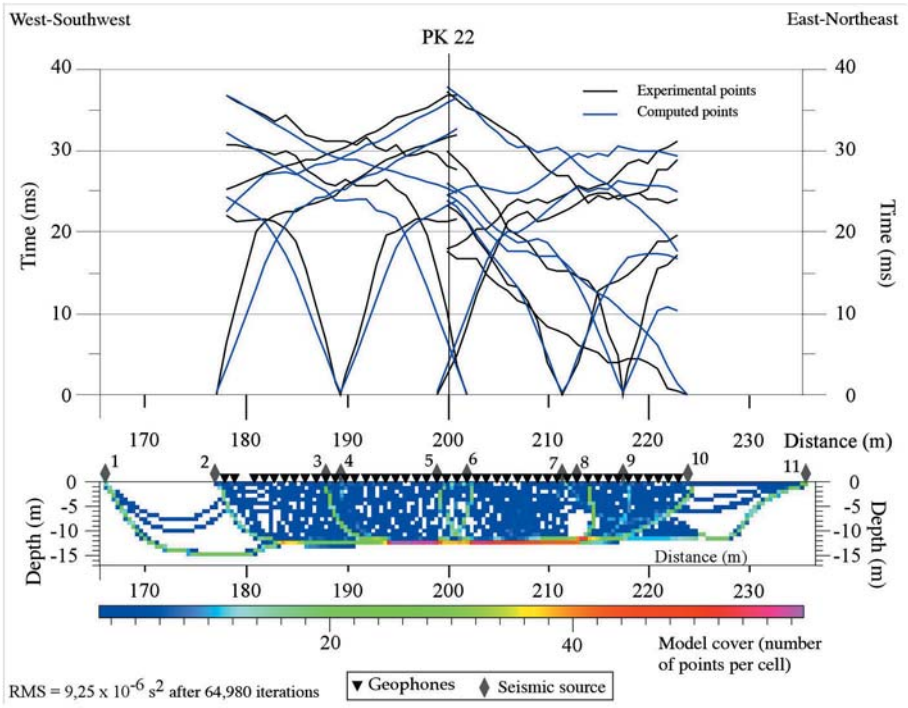

Figure 14

Comparison of experimental dromochronics (field measurements) and computed values (i.e. points determined by the software); the lower part of the figure depicts the model cover, i.e. the density of points used by the software in order to compute the model [document furnished by CETMEF]

It is also feasible to use errors in the predictions of model quality (see Fig. 14): average quadratic deviation, from a least squares perspective, between the experimental and computed measurements, graphical comparison of the experimental and computed dromochronics along with the model mesh, which indicates the number of times that a cell has been used in performing computations. The most heavily-used cells for model computation obviously correspond to the peak points selected within the computation; the observation drawn from this figure thus enables observing the computed path of seismic waves and verifying their consistency with the prospected structure.

The results obtained agree with the dromochronics and serve to highlight the gradual decrease in cover thickness heading eastward (i.e. thickness of the dam body) as well as the presence of a disturbed zone in alignment with shot no. 10 at 224 meters.

The dark dashed curve (on Fig. 13) results from an interface positioning computation by the software. The strong correlation between the summit of the compact limestone formations from borehole S3 and the seismic inversion does merit attention; this correlation indicates an interface between low-speed cover levels (500 m/sec) and high-speed substratum (4,000 m/sec) at this same depth (approx. 3 m).

Beneath this level however, the layers encountered are marls and clays not highlighted by the model (no decrease in speed may be observed at greater depths). At this point, one of the limitations of refraction seismics has been reached; this technique requires an increasing distribution in seismic speeds with depth. In the event a slow layer should get inserted between two fast layers (in this instance a marl layer between two limestone layers), the slow layer will not actually be detected [Equation 4; Keary and Brooks, 1991].

Ground-penetrating radar

Two ground-penetrating radar profiles were acquired, one over the body of the earth dam and the other on the towpath (southern bank, on the hill side) in order to derive information on this bank (Fig. 7). The general principles behind this high-output, non-destructive prospection technique have

been discussed in many articles [see for example Cariou *et al.*, 1997; Bièvre and Maurin, 2002]. The method consists in sending electromagnetic pulses inside the substratum via an antenna, at a predetermined central frequency, and then recording the return signal over a specified listening period. The waves propagate while being attenuated within the substratum and get partially reflected onto the interfaces that separate materials of varying electromagnetic properties. The amplitude of the reflections measured by the antenna is proportional to the electromagnetic contrasts between the materials positioned on both sides of the interface. The juxtaposition of the temporal signals, followed by their inversion by means of adapted mathematical processing steps (e.g. migration, waveform inversion) serve to obtain a high-resolution image of substratum geometry [Daniels, 1996]. In some cases, the unprocessed profiles provide an indication of the geometry that may be interpreted, in an initial approach, from unprocessed measurements. The profiles shown in Figure 15 take the form of a temporal section with a color scale correlated with the amplitude of the recorded signal reflections. These measurements have not been processed as part of the present scope of work. Distances are indicated with reference to PK 22, which corresponds with the abscissa x = 200 meters.

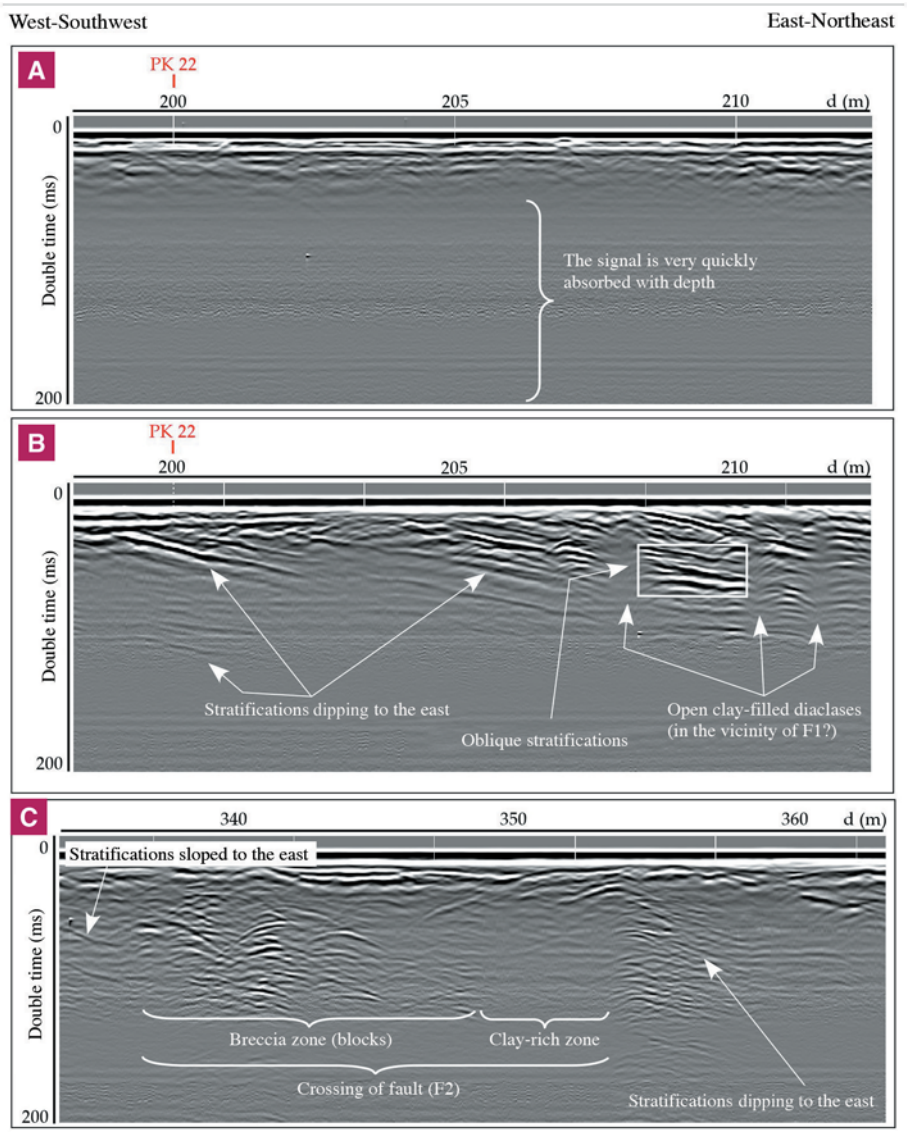

Figure 15

Ground-penetrating radar profiles acquired on the study site. The acquisition was performed using an antenna with a central frequency of 200 MHz and a sampling step of 50 scans per meter:
a. Profile at the crest of the dam at the level of PK 22
b. Profile on the hill side at the level of PK 22
c. Profile on the hill side 140 m after PK 22
The position of the profiles is indicated on Figure 7 [document furnished by CETMEF]

The equipment used for this study consists of a GSSI radar of the SIR10H type. The choice of central operating frequency for the antenna, with a monostatic configuration (the same antenna serves for both wave emission and reception), has been set to 200 MHz, for a listening period of 200 ns and a sampling rate of 50 "scans" per meter. This layout yields sufficient investigation depth (estimated at a maximum of around ten meters) and resolution for the type of geological structures targeted herein (stratifications, fractures).

An initial observation began by revealing a strong level of contrast between the two banks (see Fig. 15a). The profile derived on the southern bank (Fig. 15b), i.e. on the cut side, contains rather distinct reflections, until a listening period of up to 120 ns. The northern profile, on the dam body (Fig. 15a), only shows a few echoes beyond 50 ns. This finding is due to the nature of the dam body, which contains a sizable quantity of clays and marls that prevent the propagation of electromagnetic waves through the depth by virtue of an overly-weak resistivity. The average resistivity value of the dam body has been provided by RMT (Fig. 8) and indicates a figure of 30 Ω.m. In more general terms, it may be considered that ground-penetrating radar is not adapted to the prospection of soils with an apparent resistivity of less than about 100 ohm.m.

On the southern bank, at the level of PK 22 (Fig. 15b), the eastward dip of the layers has been highlighted and confirms the data from geological investigations. Moreover, oblique stratifications may be observed, which allows specifying that this site is located within the lower part of the Saint-Romain limestone zone (Figs. 3, 4 and 15b).

The crossing of fault F1 (Figs. 3b and 7) is not easily detectable on the radar profiles. Only a few signs of open clay-filled diaclases can actually be uncovered (Fig. 15b). From a distance of approximately 130 m after PK 22, strong reflections may be clearly identified on the southern profile (Fig. 15c). These correspond in all likelihood to the crossing of the second fault (F2; Figs. 3b and 7): a chaotic organization, strong reflections due to the presence of blocks, concentrations of electrically-conducting materials of a clay and/or marl type.

Borehole investigations

A borehole campaign using vibro-percussion and hydraulic rotation (VPHR) has enabled specifying the nature and state of the embankments as well as the Jurassic formations [Rousseau and de Sambucy, 1993]. These drillings are destructive and commonly referred to as "continuous core sampling"; they serve to obtain detailed and precise borehole section cuts with a high level of output (up to several hundreds of meters per day). This set of drillings, carried out on the dam valley side, have been presented in Figure 16 (localization from a plane perspective on Figure 7). The cuts

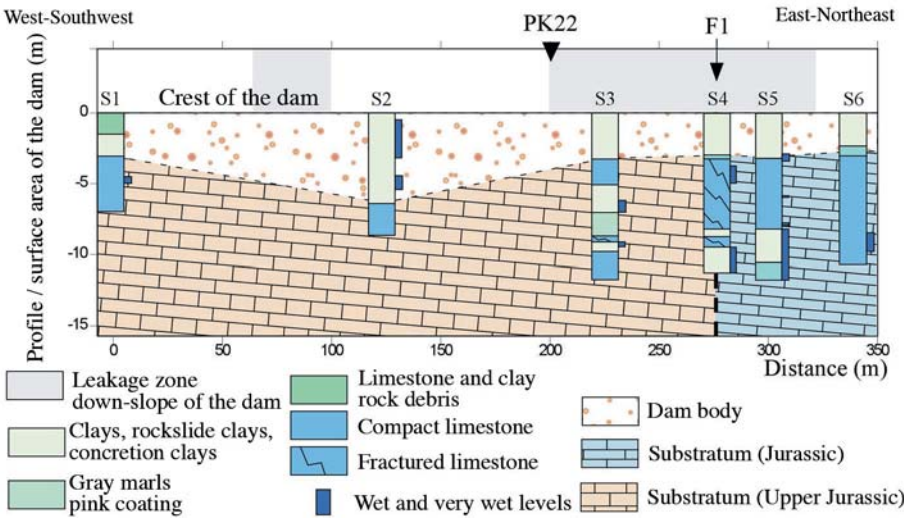

Figure 16

Borehole investigations and geotechnical extrapolation [modified after Rousseau and de Sambucy, 1993]. The position of the probes is indicated on Figure 7.

obtained indicate the alternations of limestone and Jurassic marl positioned underneath a cover layer that corresponds to the earth dam embankment. The average depth of the base of the dam body is approximately 2.5 m, except at the level of borehole S2, where it reaches about 6 m. This spot is also the only one where humid to very humid layers were observed within the dam body. These layers exist at a height lower than that of the embankment base, i.e. the water encountered is found within the Jurassic formations in place.

At the level of borehole S4, the entire series of limestone layers encountered is fractured. This observation corroborates that of the geological map, PECSA, refraction seismics and ground-penetrating radar, i.e.: fault F1 crosses in the vicinity of this borehole (Figs. 3 and 7), which explains the drops recorded in apparent resistivities (Figs. 10 and 11a), in the same way as the presence of fault F1 has been confirmed through detection by both seismic refraction (Fig. 13) and ground-penetrating radar (F1 and F2, Figs. 15b and 15c).

Aquatic Profiling Spontaneous Potential (SP)

The method of electrical spontaneous potential (SP) consists in a non-destructive geophysical prospection technique, classically employed on ground applications as point-specific instrumentation. The objective herein was to develop a high-output aquatic streaming method in order to characterize earth dam leakage.

This method is based on measurements of the natural electrical potential generated in a variety of ways within the substratum by means of electrochemical interactions taking place between minerals, electro-kinetic processes, and a temperature or pore pressure gradient. These processes induce a flux of ions and thus the creation of a potential difference (pd): this is the potential created by hydraulic flow within the soil, also called electro-filtration potential or electro-kinetic potential, which gets used primarily in civil engineering applications. Put briefly, the pd measured between a downstream point and an upstream point within the circulation zone is explained by the polarization resulting from the coupling between the circulating ionic solution and the double electrical layer (the so-called "Helmoltz layer") of the capillary walls of porous media [MacInnes, 1961; Corwin and Hoover, 1979]. In the presence of a neutral or basic water, the potential is positive, while a leakage zone generates a negative anomaly, and a rise in the impermeable zone generates a positive anomaly [Aubert, 1997].

The value of the electro-kinetic potential created is given by Equation (6) [Corwin and Hoover, 1979]:

$$V = \frac{\rho \varepsilon \zeta}{4\pi\eta} \Delta P \qquad (6)$$

with:

- V = electro-kinetic potential (volts),
- ρ = resistivity of the solution (Ω.m),
- ε = dielectric constant of the solution (F/m),
- ξ = pd through the double Helmoltz layer (V), also called the zeta potential,
- ΔP = pressure difference along the path traveled by the fluid (Pa),
- η = dynamic viscosity of the solution (Pa.s).

Ground SP is a longstanding technique: it has been used ever since the first half of the 19th century for identifying copper sulfate deposits. Since then, this method, commonly employed for localizing mineral deposits [Sato and Mooney, 1960; Corwin, 1976], has been developed for: studying fluid circulation within substrata [Corwin and Hoover, 1979; Aubert, 1987], geotechnical applications [Al Saigh et *al.*, 1994; Bogoslovsky and Ogilvy, 1970; Ogilvy et *al.*, 1969], and more fundamental geological and geodynamic applications [Aubert et *al.*, 1991; Trique et *al.*, 2000; Hovhanissian et *al.*, 2000; Jouniaux and Pozzi, 1997].

The equipment includes a cable fitted with four unpolarizable electrodes with fixed spacing (gradient device), which allows defining two measurement dipoles. This streamer is dragged on the canal floor and connected to a laptop computer that serves as a millivoltmeter, by means of a data acquisition card and adapted software, along with a data storage unit (Fig. 17). This set-up is mounted aboard the boat. The resulting prospection method is relatively inexpensive, very simple to implement and capable of generating up to several kilometers of data acquisition per day.

Three profiles derived on the towpath side have been presented (Fig. 18; localization of the profiles on Figure 7). Measurements were acquired using electrodes with a spacing of 5 m and 15 m respectively and with two path directions (east-to-west: EW, or west-to-east: WE) and two periods (one series during July and another during August).

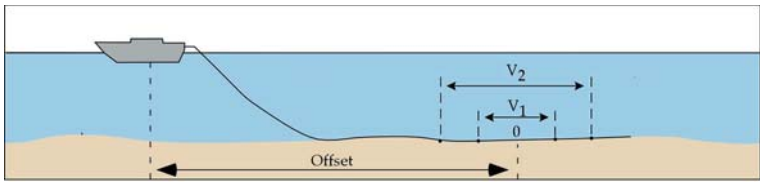

Figure 17

Device for measuring the aquatic spontaneous potentials
V_1: difference in potential measured by the electrodes with a spacing of 5 m
V_2 : difference in potential measured by the electrodes with a spacing of 15 m
Offset: distance between the boat and the center of the measurement device (0)

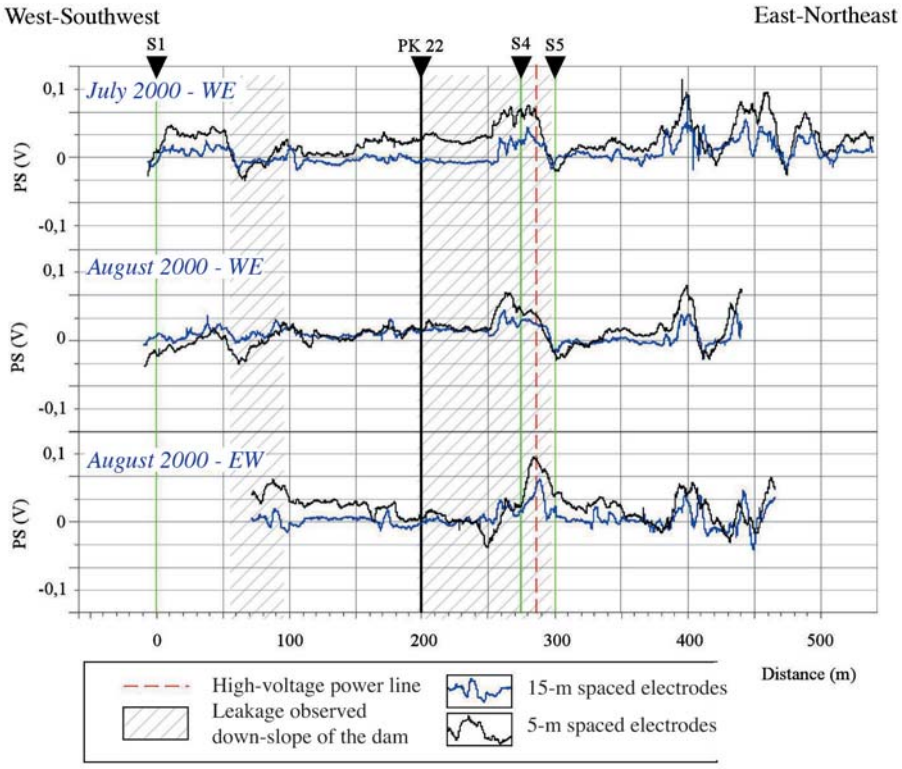

Figure 18

Aquatic spontaneous potential (SP) profiles derived on the canal towpath side [Norgeot, 2000; Bièvre and Norgeot, 2003].
The measurements were performed using 5 m and 15 m electrodes spacings with two path directions (east-to-west: EW, or west-to-east: WE) and over two periods (July 2000 and August 2000). The position of the profiles has been indicated on Figure 7.

An initial analysis of results shows that both positive and negative anomalies are detected and that these are located at the same places on the profiles. Since data acquisitions had been performed in both directions and during two distinct periods, it may be observed that the system allows for a high level of measurement repeatability and that the recorded anomalies correspond to a variation in physicochemical parameters at the level of the electrodes.

An initial negative anomaly has been identified at the level of the first leakage zone, on the WE profiles (between 0 and 50 m; Fig. 18), with a pd showing an amplitude of approximately -100 mV. The lateral extension of this anomaly is quite substantial, on the order of 20 meters. Another negative anomaly is observed, exclusively on the EW profile, at the level of the second leakage zone (x = 250 m, 5-m electrodes; Fig. 18), with a negative potential of an amplitude in excess of 100 mV and a lateral extension of approximately 20-25 m. The three profiles all display a highly-positive anomaly

at the end of the second leakage zone with considerable lateral extension. Other anomalies, quite sizable in both the negative and positive directions, are also observable at the end of the profile between abscissas of 350 and 450 meters.

Theory proposes that the anomalies generated by leakage (draining zone from the canal until reaching the base of the earth dam) are of negative potential [Aubert, 1997]. Two anomalies of this type have been identified on SP profiles at the level of leakage zones down-slope of the dam (Fig. 18). Their lateral extension however proves to be quite significant (20 to 25 m). Visual observations inside the canal [ISL, 1994] indicate that the magnitude of leaks lies on the order of several tens of centimeters at most (inframetric in any case).

Other anomalies, positive this time, have been detected (end of the second leakage zone, x = 250 to 300 m; end of the profile, beginning at x = 380 m; Fig. 18). These would correspond to a neutral or basic water or perhaps to a rise in an impermeable layer [Aubert, 1997].

Furthermore, a comparison with data found in the literature [Ogilvy et *al.*, 1969; Al-Saigh et *al.*, 1994; Bogoslovsky and Ogilvy, 1970] suggests that the amplitude of detected anomalies is high (reaching up to a hundred mV), while they barely surpass several tens of mV in the research examined.

Discussion of results

Depending on the geological data available, the carbonated Bathono-callovian and Oxfordian formations composing the substratum are organized into thin strips, with a stratification dipping towards east-southeast and a sizable level of fracturing throughout the entire block (Figs. 3 and 4). Moreover, according to physicochemical readings (Figs. 5 and 6), these strata contain at least one water table that circulates via fractures and/or along stratification planes.

Mechanical drillings reveal the existence of wet zones within the in situ carbonated Jurassic formations, below the embankment that constitutes the left bank (on the towpath side) of the canal (Fig. 16). It would also appear that beginning at PK 22, the canal is built in alignment with a fault (F1) that it subsequently partially follows (Fig. 3b).

The comparison of mechanical drillings and geophysical measurements shows a good overall level of agreement among the various methods. It is now possible to proceed with decomposition into three zones: the first from the beginning of the PECSA profiles until reference x = 40 m, the second up until PK 22, and the third to the end of the prospection zone. It also becomes possible to position the crossing of accidents F1 and F2 on the basis of geophysical data (Fig. 19a).

First zone: From the start of profiles to abscissa x = 40 m

The RMT data are rather easy to correlate with the mechanical drillings for high frequencies, i.e. the surface layers (Figs. 8 and 16). For lower-frequency measurements, the first part of the profile exhibits a logical correlation with apparent resistivity values that gradually decrease along the profile, whereas the top of the substratum dips eastward and the volume of the more conductive materials increases within the first slice of substratum. The electrical organization of the ground (conductive dam body located on a more highly-resistive substratum) influences the measurement at 162 kHz: the electrical current circulates more easily within the conductive facies. As such, local organization tends to concentrate the electrical current within the upper part of the substratum and limit its depth penetration.

A comparison of PECSA with the results from both mechanical drillings and visual observations of leakage zones along this first survey zone may seem a bit puzzling (Figs. 10, 11 and 16): the limestone is reached at 3 m in borehole samples (S1) and does not apparently display extensive wet zones (a single intake at 4.4 to 5.2 m). Below this point, apparent resistivities remain small and are difficult to explain should these layers correspond with massive limestone. A PECSA testing campaign conducted on behalf of the local Public Works Office in the Saône-et-Loire department (DDE 71) did however reveal a set of readings comparable to the profiles, which indicates the high level of measurement repeatability [Bièvre, 2003]. In reference to structural data, it is known that the in situ carbonated formations composing the substratum dip to the east and that fluids may indeed circulate through these formations. It thus proves possible that the leakage zone observed at the beginning of the profile has resulted in part in flow emanating from the water table. Its origin is hence located more to the west with respect to its outfall at the base of the dam and this water passes underneath the canal: this observed zone of low resistivity can be explained by a circulation of water in part

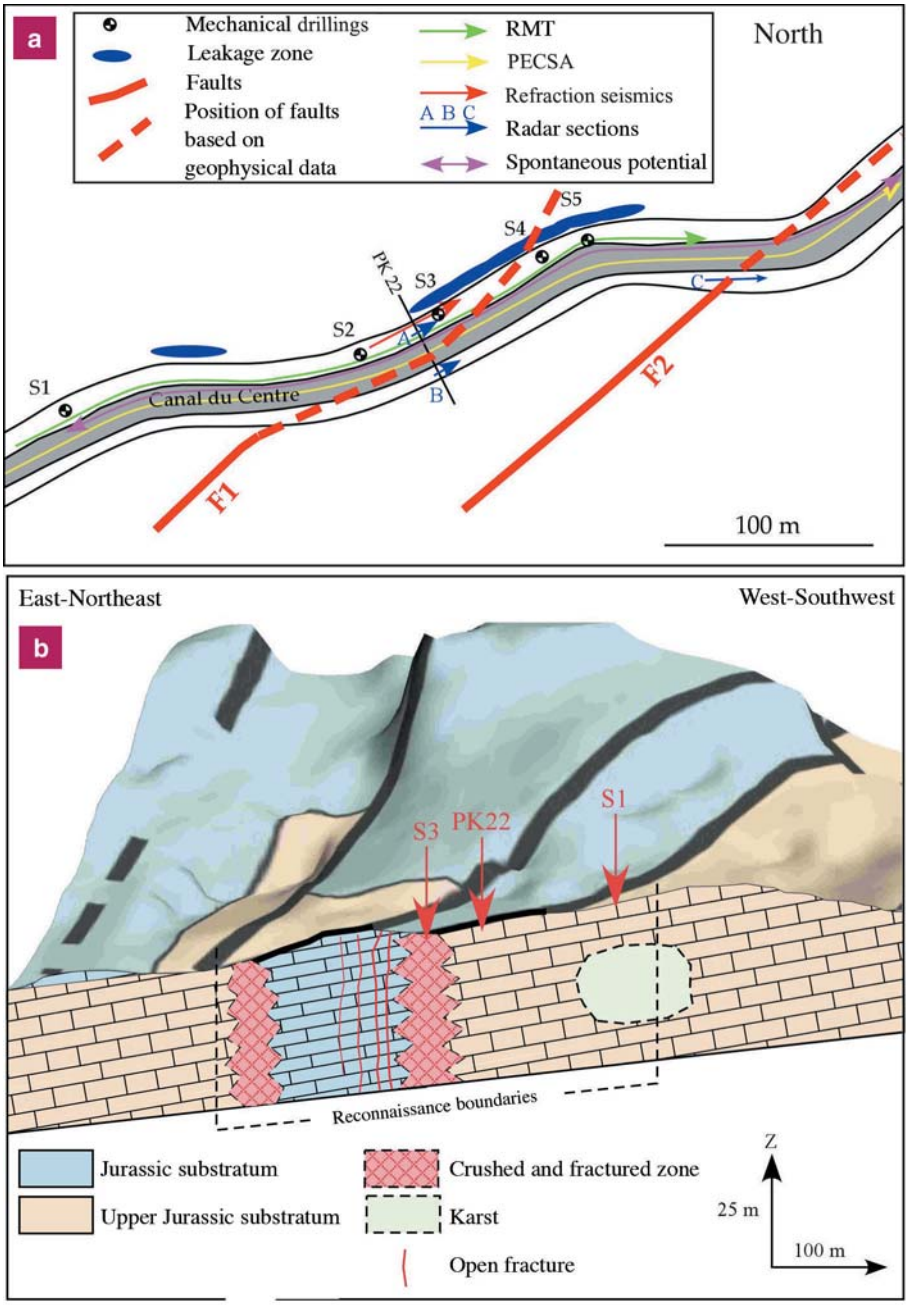

Figure 19

Geological interpretation of the geophysical data:
a. Position of faults F1 and F2 underneath the canal and the earth dam based on the synthesis of geophysical data
b. Geological synthesis of the study sector

within the substratum. It is probable that the low resistivity values signify here a zone of fairly intense karstification. This hypothesis has been strengthened by the inconsistency over this sector of apparent resistivity values (Figs. 10 and 11), which suggests sizable lateral heterogeneity. These observations in all likelihood indicate a substratum with weak mechanical characteristics.

Lastly, these observations also allow forwarding that the 162-kHz RMT investigation depth at this particular spot is limited to 6-7 m, with the mechanical probes indicating the presence of compact limestone to a depth of at least 6 m (Figs. 8 and 16). The karst is most likely situated at a greater depth.

Second zone: From abscissa x = 40 m to PK 22

The increase in thickness of the clayey dam cover layer heading eastward, which progresses from approximately 2 m (S1) to 6 m (S2), at the same time that the wet zones within the cover layers become extensive, serves to induce a drop in apparent resistivity values at low-frequency RMT, which agrees with both refraction seismics results and the analysis of mechanical drillings (Figs. 8, 13 and 16). The 603-kHz RMT remains stable however, which demonstrates that at this frequency, the layers located below 2 m do not exert any influence on measurements. This finding also agrees with the estimation of investigation depth obtained for this frequency (d = 2 m; see section "The radio-magnetotelluric technique"), which frames the analysis exclusively at the dam body. No anomaly exists on low-frequency RMT profiles at the level of the first leakage zone at the dam base (Fig. 8).

This zone displays a logical correlation between a borehole that reaches the limestone at around 6 m (S2) and a vertical distribution of the PECSA apparent resistivities, pointing to layers that quickly become more highly resistive at the same time as penetrating the compact limestone layers (Figs. 10, 11 and 16).

Third zone: From PK 22 to the end of profiles

From PK 22 forward, this portion constitutes a second leakage zone down-slope of the earth dam. The boreholes show sizable lateral variability (see Fig. 16); they indicate a substratum composed of layers in which fractured marl, clay and limestone all alternate. Furthermore, the number of wet zones in the boreholes is high, as is the number of leaks observed at the base of the dam. This position coincides with a crushed and highly-fractured zone, which corresponds with the crossing of fault F1 beginning at the base of the dam, located at a depth of approximately 2.5 m.

RMT does not expose these variations (Fig. 8). The analysis of PECSA profiles reveals a general sinking of the resistive layers as of PK 22 (Figs. 10 and 11). Comparison with borehole data suggests that the anomaly is situated in alignment with a fault zone (Fig. 16). The end of the profile shows a gradual rise in resistive layers ("dipping of electrical facies"; Fig. 11). It may be considered that a gradual transition is being made to less fractured and more highly-compact formations, in which water is circulating to a lesser extent.

Refraction seismics highlighted the crossing of a fault, in the vicinity of borehole S4 (Fig. 13), which is entirely corroborated by geological information (Fig. 3).

This geological accident has also been detected using radar on the profile generated for the southern bank (see Fig. 15b). According to the interpretation of these profiles, it would appear that open fractures filled with clay exist near the primary axis of this accident, which explains the gradual rise in PECSA apparent resistivities at this particular site.

These anomalies on the geophysical recordings (PECSA, refraction seismics, ground-penetrating radar) are in perfect harmony with geological information (Fig. 3b) and enable placing the path of the primary axis of fractures F1 and F2 under the canal and dam body (Fig. 19a).

Geological model and integration of SP data

An analysis of the entire set of data acquired gives rise to a geological organization model for the purpose of interpreting SP measurements (Figs. 19a and 19b). According to this study, it seems that the leaks observed down-slope of the earth dam only partially correspond with a supply fed by leaks observed in the canal. It also appears that the substratum acts as the seat for a more intense circulation of fluids, which serves to incite the geological organization: lithology favorable for karstification, stratification generally dipping to the east, and more pronounced fracturing patterns in the carbonated formations. It is thus possible that the leaks existing within the canal do not directly reach the area down-slope of the dam, but rather the substratum, which would agree with the findings of Fleury and Gélard [1983] regarding the circulation of groundwater. As such, the SP anomalies recorded, yet which were not correlated with leakage at the base of the dam, can potentially be explained. Moreover, infiltrations were recorded on the right bank [ISL, 1994]; these convey groundwater with distinct physicochemical characteristics (pH, ion content, highly-localized resistivity variations; Figs. 5 and 6) into the canal. These infiltrations may also lie at the origin of anomalies recorded in SP, while not being easily correlated with leakage down-slope of the dam. Observation of the profiles (Fig. 18) has indicated quite distinctly the strong repeatability of these measurements, which

would suggest that the anomalies recorded are due to a modification in physicochemical conditions at the level of the electrodes. The strongly-positive anomalies (between S3 and S4 on Figure 18), as well as the mixed positive/negative anomalies observable at the end of the profile (Fig. 18, beginning at abscissa 350 m), which all feature sizable lateral extension, are located in exact alignment with the crossing of the two faults noted on the geological map (Fig. 3b) and whose position has been confirmed by both geophysical techniques (PECSA, Figs. 10 and 11; refraction seismics, Fig. 13; ground-penetrating radar, Fig. 15) and mechanical probes (Fig. 16). The boreholes also revealed the considerable circulation of water at these specific spots. It would thus be possible to propose that the SP signals recorded result from groundwater infiltration and/or water circulation at these sites. This zone would also feature the infiltration of groundwater into the canal and leakage from the canal towards the area down-slope of the dam.

Conclusion

Various non-destructive geophysical prospection methods have been tested on the Canal du Centre for the purpose of knowing their possibilities and limitations within the scope of earth dam prospection. This work has demonstrated the overall ease with which such techniques may be employed in the field; for the majority of techniques, the output provided was substantial.

The methods implemented have contributed complementary information, depending on whether they focus on the earth dam or the substratum. Their results agree well with geological observations made (mapping, boreholes) and enable clarifying certain points not directly observable in the field (e.g. position of a fault beneath a recent cover layer, karstification indices). The results acquired thanks to the various techniques employed in this study reveal the benefit of relying upon an approach that makes use of several methods (physical measurements on water, in-depth geological investigations, geophysical methods) in order to master the full array of influential parameters.

Another general finding from this study is the tremendous complexity of the site, which complicates localization, at the canal level, of leaks observed down-slope of the earth dam. Several parameters are involved and these intimately mingle the respective roles of the canal and the water table.

References

ABBOTT R.E., LOUIE J.N., CASKEY S.J., PUPLLAMMANAPPALLIL S., Geophysical confirmation of low-angle normal slip on the historically active Dixie Valley fault, Nevada, *Journal of Geophysical Research*, **106, 2001,** pp. 4169-4181.

AL-SAIGH N.H., MOHAMMED Z.S., DAHHAM M.S., Detection of water leakage from dams by self-potential method, *Engineering Geology*, **37,** 2, **1994,** pp. 115-221.

ARCHAMBAULT C., **1997.** Résultats non publiés.

AUBERT M., La méthode des potentiels électriques spontanés (PS) en hydrogéologie, *Bull. Soc. Géol. France*, **8,** t. III, n° 5, **1987,** pp. 953-956.

AUBERT M., Application de la mesure des potentiels électriques de polarisation spontanée (PS) à la reconnaissance des formations superficielles, *Livre des résumés, I^er^ Colloque GEOFCAN*, 11-12 septembre **1997,** Bondy.

AUBERT M., DANA I.N., DUPUIS J.-C., Application de la méthode de polarisation spontanée à la découverte des circulations d'eau souterraine en terrain volcanique, *C. R. Acad. Sc. Paris*, **312,** série II, n° 3, **1991,** pp. 325-330.

BIÈVRE G., *Poursuite du développement de la méthode de Polarisation Spontanée – Couplage avec une prospection géoélectrique aquatique (PECSA)*, Rapport de recherche LCPC, n° 1AEP21, **2002.**

BIÈVRE G., *Prospection géoélectrique aquatique sur le Bief de Chagny-Première partie : rapport de prospection géophysique*, Rapport d'étude LRPC d'Autun n° 15697, **2003.**

BIÈVRE G., MAURIN P., Évaluation d'un radar géologique sur le site-test géophysique du LCPC à Nantes (France), *Bulletin des laboratoires des Ponts et Chaussées*, **240, 2002,** pp. 73-85.

BOGOSLOVSKY V.A., OGILVY A.A., Natural potential anomalies as a quantitative index of the rate of seepage from water reservoirs, *Geophysical Prospecting*, **18, 1970,** pp. 261-268.

CAGNIARD L., Basic theory of the magneto-telluric method of geophysical prospecting, *Geophysics*, **18, 1953,** pp. 605–645.

CARIOU J., CHEVASSU G., CÔTE Ph., DÉROBERT X., LE MOAL J.-Y., Application du radar géologique en génie civil, *Bulletin des laboratoires des Ponts et Chaussées*, **211, 1997,** pp. 117-131.

CORWIN R.F., Offshore use of the self-potential method, *Geophysical Prospecting*, **24, 1976,** pp. 79-90.

CORWIN R.F., HOOVER D.B., The self-potential method in geothermal exploration, *Geophysics*, **44** (2), **1979,** pp. 226-245.

DANIELS D.J., *Subsurface-penetrating radar*, The Institution of Electrical Engineers, London, UK, **1996,** 300 pages.

FAUCHARD C., MÉRIAUX P., *Méthodes géophysiques et géotechniques pour le diagnostic des digues de protection contre les crues – Guide pour la mise en œuvre et l'interprétation*, Projet National CriTerre, CEMAGREF Éditions, **2004,** 150 pages.

FLEURY R., GÉLARD J.-P., *Notice explicative de la feuille Chagny à 1/50 000*, Éditions du BRGM, Orléans, **1983.**

GUINEAU B., Exemples d'applications de la méthode magnétotellurique de prospection géophysique à l'étude de structures ou de formations géologiques situées sous un très faible recouvrement, *Geophysical Prospecting*, **2, 1975,** pp. 104-123.

HAGEDOORN J.G., The plus-minus method of interpreting seismic refraction sections, *Geophysical Prospecting*, **7, 1959,** pp. 158-182.

HAWKINS L.V., The reciprocal method of routine shallow seismic refraction investigations, *Geophysics*, **26, 1961,** pp. 806-819.

HOLLIER-LAROUSSE A., *Contribution à la valorisation d'une méthode géophysique électromagnétique utilisée en géophysique appliquée de subsurface : la radio magnétotellurique*, Diplôme d'ingénieur CNAM, Paris, **1997,** 217 pages.

HOVHANISSIAN G. M., POZZI J.-P., BERNARD P., Les signaux transitoires PS sur des échantillons saturés et non saturés, *Livre des résumés, Réunion spécialisée de la S.G.F.*, 16 mars **2000,** Paris.

ISL Bureau d'ingénieurs conseil, *Canal du Centre-Bief 23-24 Méditerranée. Rapport d'étude diagnostic d'étanchement*, Rapport ISL n° VNF-017 du 26 décembre **1994,** Paris.

JOUNIAUX L., POZZI J.-P., Laboratory measurements anomalous 0.1-0.5 Hz streaming potential under geochemical changes : implications for electrotelluric precursors to earthquakes, *Journal of Geophysical Research*, **102,** n° B7, **1997,** pp. 15335-15343.

KEARY P., BROOKS M., *An introduction to geophysical exploration*, Blackwell Scientific Publications, Oxford, **1991,** 254 pages, 2nd Edition.

LAGABRIELLE R., The effect of water on direct current resistivity measurement from the sea, river or lake floor, *Geoexploration*, **21, 1983,** pp. 165-170.

LAGABRIELLE R., La prospection électrique par courant continu en mer, *Bulletin de liaison des Laboratoires des Ponts et Chaussées,* **132, 1984,** pp. 5-11.

LAGABRIELLE R., CHEVALIER M., Prospection électrique par courant continu en site aquatique, *Bulletin de liaison des Laboratoires des Ponts et Chaussées*, **171, 1991,** pp. 57-62.

LAGABRIELLE R., HOLLIER-LAROUSSE A., Les deux types d'informations contenues dans les profils de magnétotellurique artificielle : exemple d'application à la prospection archéologique, *Bulletin de liaison des Laboratoires des Ponts et Chaussées*, **137, 1985,** pp. 17-24.

LAGABRIELLE R., TEILHAUD S., Prospection de gisements alluvionnaires en site aquatique par profils continus de résistivité au fond de l'eau, *Bulletin de liaison des Laboratoires des Ponts et Chaussées*, **114, 1981,** pp. 17-24.

MACINNES D.A., *The principles of electrochemistry*, Dover Publishing Co, New York, **1961.**

MCNEILL J.D., LABSON V., Geophysical mapping using VLF radio fields, *In* : NABIGHIAN M.N. (Ed.), *Electromagnetic methods in applied geophysics*, Soc. Expl. Geophys., **2,** part B, **1991,** pp. 521-640.

MÉRIAUX P., ROYET P., CÔTE P., HOLLIER-LAROUSSE A., FRAPPIN P., Méthodes de reconnaissance géophysique à grand rendement pour les digues de protection contre les crues, *Livre des résumés, IIe Colloque GEOFCAN*, Orléans, septembre **2001.**

NORGEOT C., *Test de la Polarisation Spontanée pour la recherche de fuites dans les digues*, Mémoire de DESS de géophysique appliquée, Université Paris VI/LRPC d'Autun, **2000.**

OGILVY A.A., AYED M.A., BOGOSLOVSKY V.A., Geophysical studies of water leakages from reservoirs, *Geophysical prospecting*, **17, 1969,** pp. 36-62.

PULLAMMANAPPALLIL S.K., LOUIE J.N., A Generalized Simulated-Annealing Optimization for Inversion of First-Arrival Times, *Bull. of the Seismological Society of America*, **84,** n° 5, **1994,** pp. 1397-1409.

PULLAMMANAPPALLIL S.K., LOUIE J.N., A combined first-arrival travel time and reflection coherency optimisation approach to velocity estimation, *Geophysical Research Letters*, Vol. **24,** n° 5, **1997,** pp. 511-514.

RAT P., *Bourgogne Morvan*, Guide Géologique Régional, 2e édition, Masson, Paris, 1986.

ROUSSEAU F., DE SAMBUCY, *Rapport d'étude géotechnique sur le Bief 23-24 Méditerranée du canal du Centre*, Rapport LRPC d'Autun n° 90-2502, **1993.**

SATO M., MOONEY H.M., Electrochemical mechanism of sulfide self-potentials, *Geophysics*, **25, 1960,** pp. 226-249.

TRIQUE M., PERRIER F., FROIDEFOND, AVOUAC J.-P., Étude de variations de potentiel électrique associées à des variations de niveau de lac, *Livre des résumés, Réunion spécialisée de la SGF*, 16 mars **2000,** Paris.

ZOHDY A.A.R., A new method for the automatic interpretation of Schlumberger and Wenner sounding curves, *Geophysics*, **54,** n° 2, **1989,** pp. 245-253.